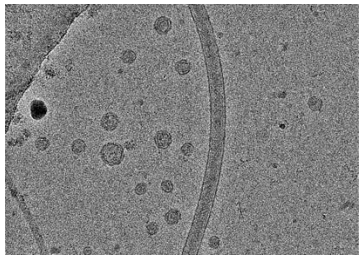

21,747 movies

Motion Correction
CTF Estimation

Filament tracer

3,059,499 particles

2D classification

Sheathed filament

Unsheathed filament

76,818 particles

443,577 particles

Helical refinement
Local CTF refinement
3D classification

Helical refinement
Local CTF refinement
3D classification

72,779 particles

439,378 particles

Local refinement

Local refinement

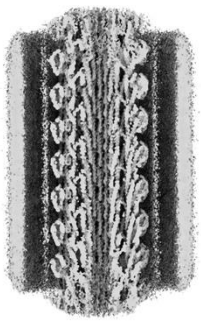

3.6 Å

High contour

Low contour

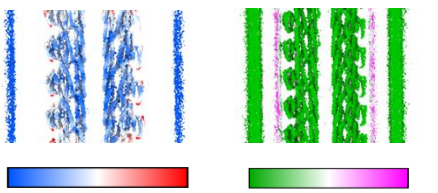

Resolution (Å)

3.2 Å

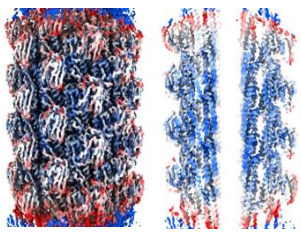

Resolution (Å)

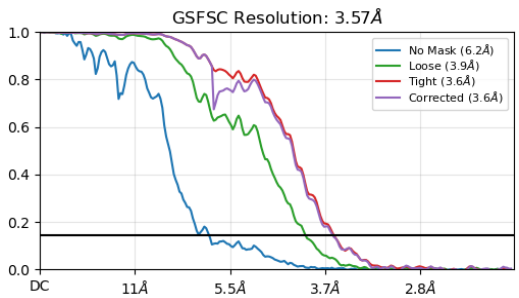

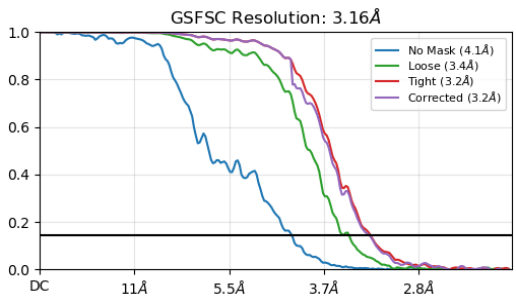

Figure S1. **Cryo-EM data processing workflow of the sheathed and the unsheathed flagellar filament of *V. alginolyticus*.** The various steps used for processing are shown, with local resolution and FSC curves shown for both structures.

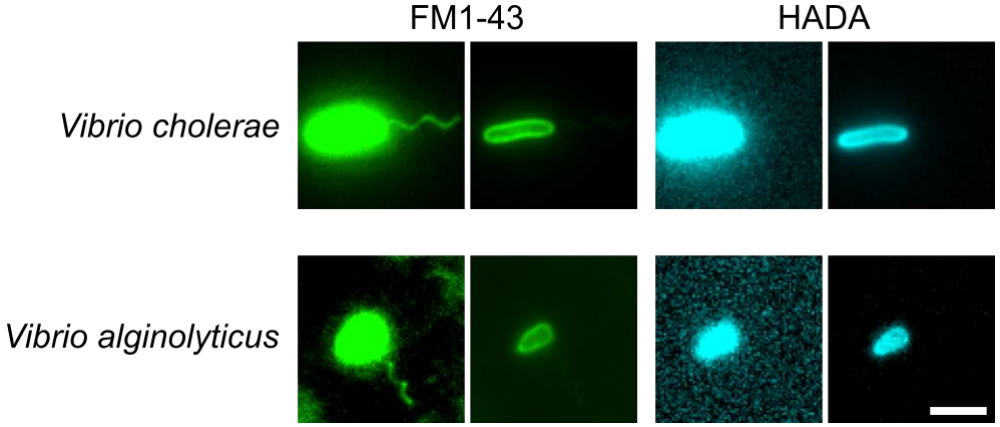

Figure S2. The flagellar sheath does not contain peptidoglycan. Representative fluorescence microscopy images of *V. cholerae* and *V. alginolyticus* cells stained with FM1-43 (green) to visualise the outer membrane and flagellar sheath, and the fluorescent D-amino acid HADA (cyan) to label peptidoglycan. Scale bar, 3 µm.

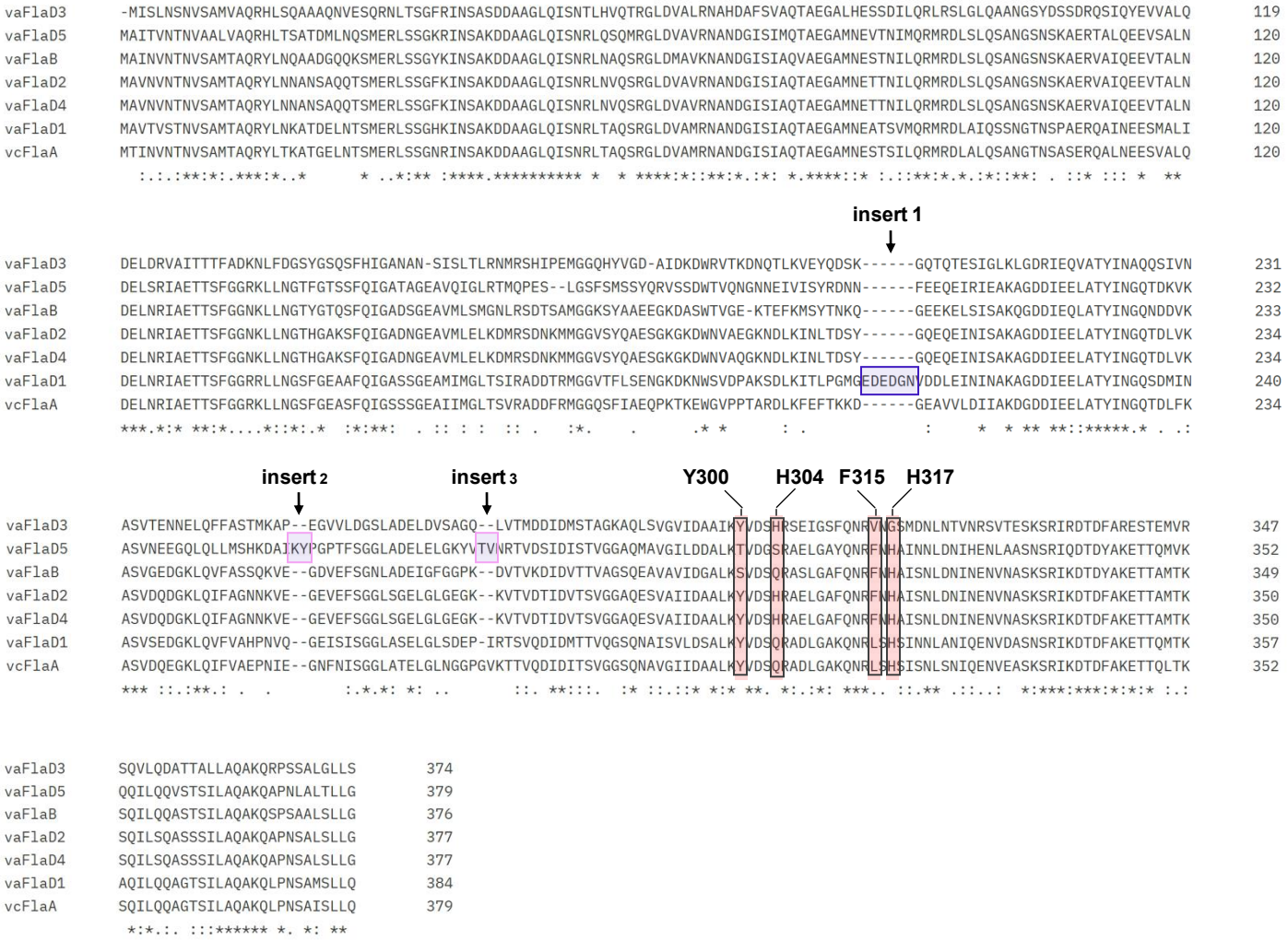

Figure S3. Multiple sequence alignment of the *V. alginolyticus* flagellin sequences. The three inserts, and four residues, involved in identifying the correct flagellin in our filament structure are indicated.

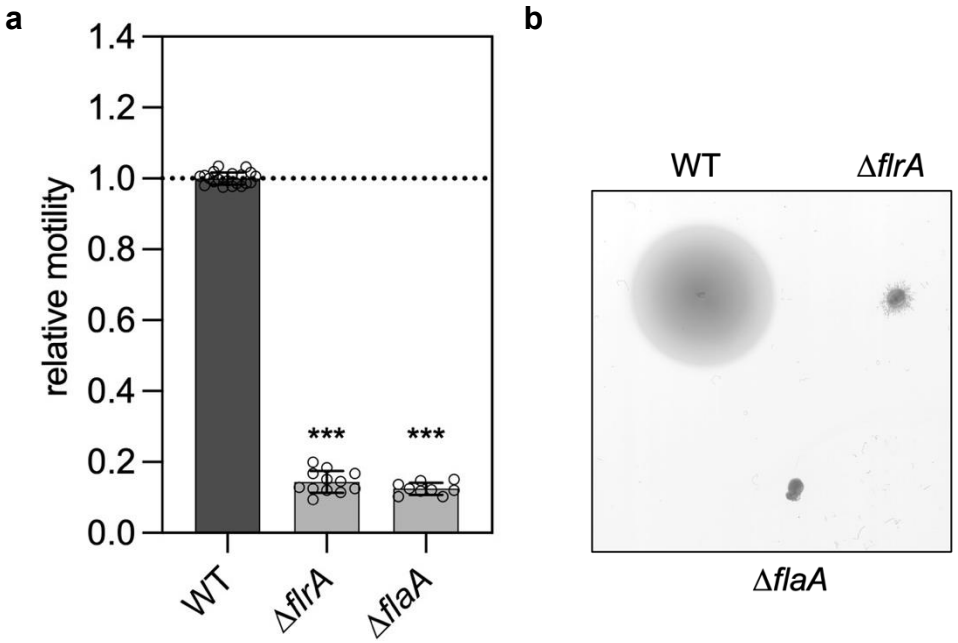

Figure S4. FlaA is the main flagellin of the *V. cholerae* flagellar filament. a, Relative motility of *V. cholerae* Δ*flrA* (non-motile control) and Δ*flaA* (essential flagellin) mutants, analyzed using soft-agar motility plates after 6-8 h incubation at 37 °C. Motility halos were measured using Fiji and normalized to the WT. Bar graphs show mean ± SD from ≥3 biological replicates with individual data points. **b,** Representative swimming halos for the strains shown in a. Statistical analysis was performed using one-way ANOVA followed by Dunnett's multiple comparisons test (GraphPad Prism). *, $p < 0.05$; **, $p < 0.01$; ***, $p < 0.001$; ns, non-significant.

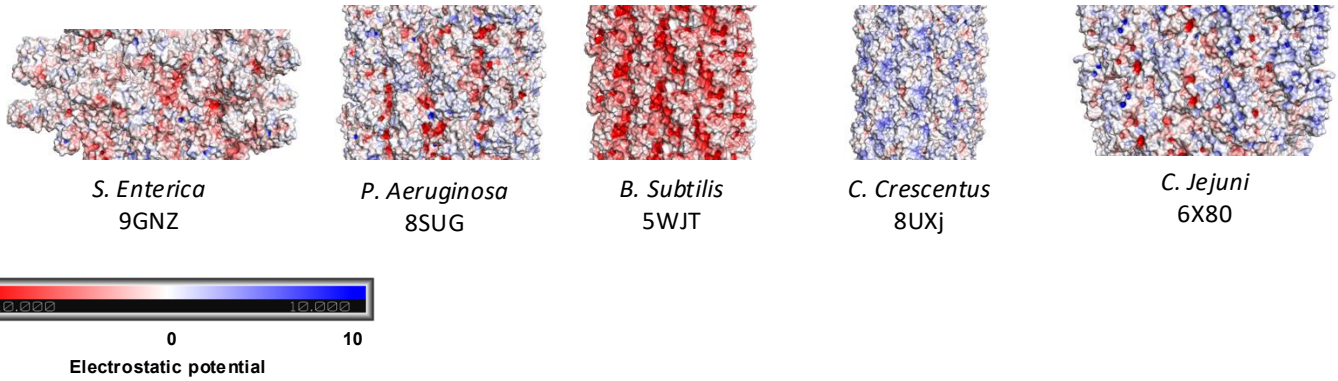

Figure S5. Electrostatic surface of flagellar filaments across bacteria. A surface representation of the flagellum filament structure for divergent bacterial species are shown, colored by electrostatic potential (in kT/e). No obvious trend is observed, with most having a largely neutral surface, with the exception of the *B. subtilis* filament which is electronegative.

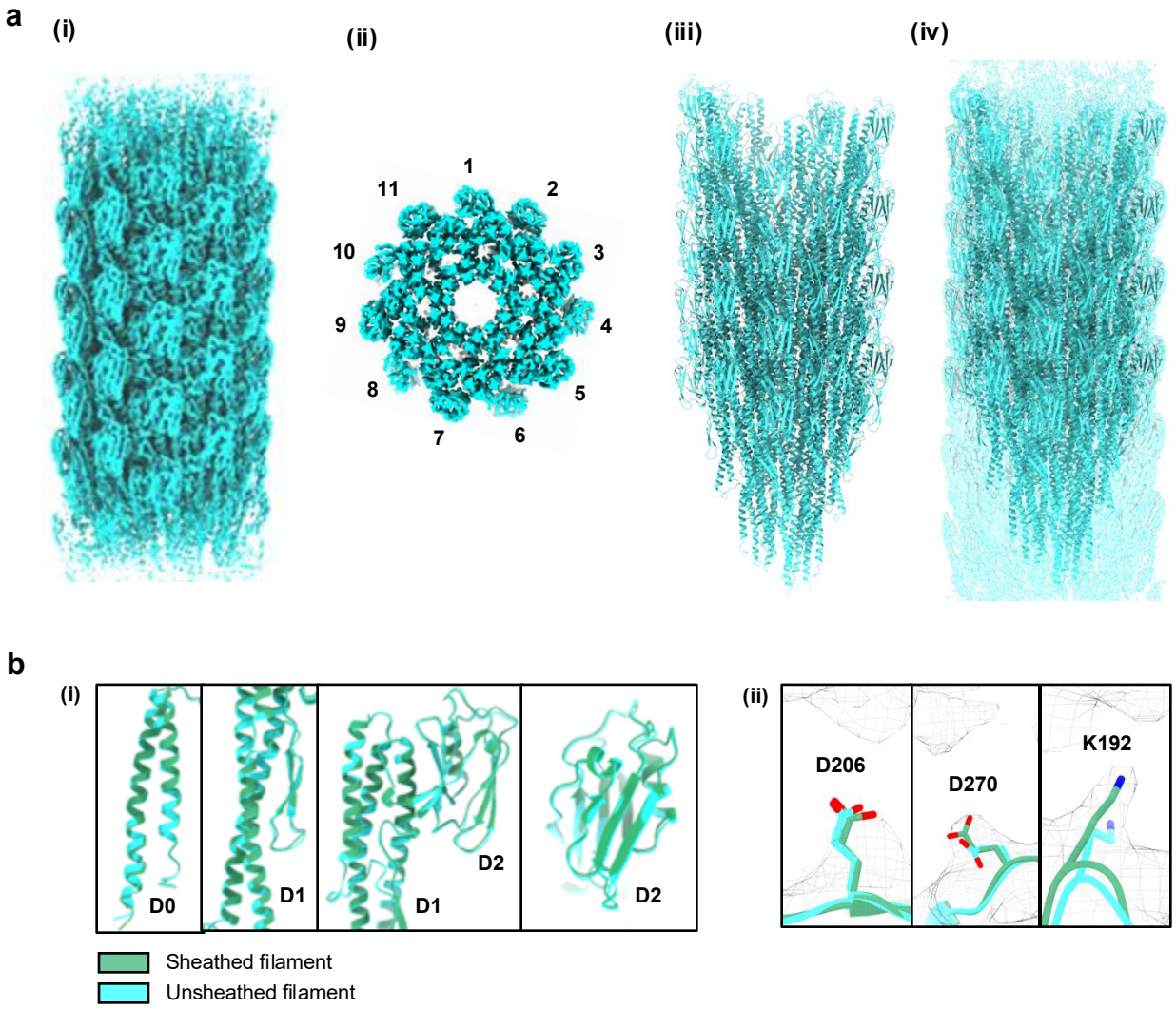

Figure S6. Structure of unsheathed filaments from *V. alginolyticus*. a, Cryo-EM map of unsheathed filament from the side (i) and top (ii), and corresponding atomic model (iii) fitted into the map (iv). **b**, Comparison of the structure of the V. alginolyticus flagellum filament, with (green) and without (cyan) its sheath. No significant differences are identified, at the backbone level, for any of the domains (i); very minor differences are found to the side-chain of residues facing the membrane (ii).

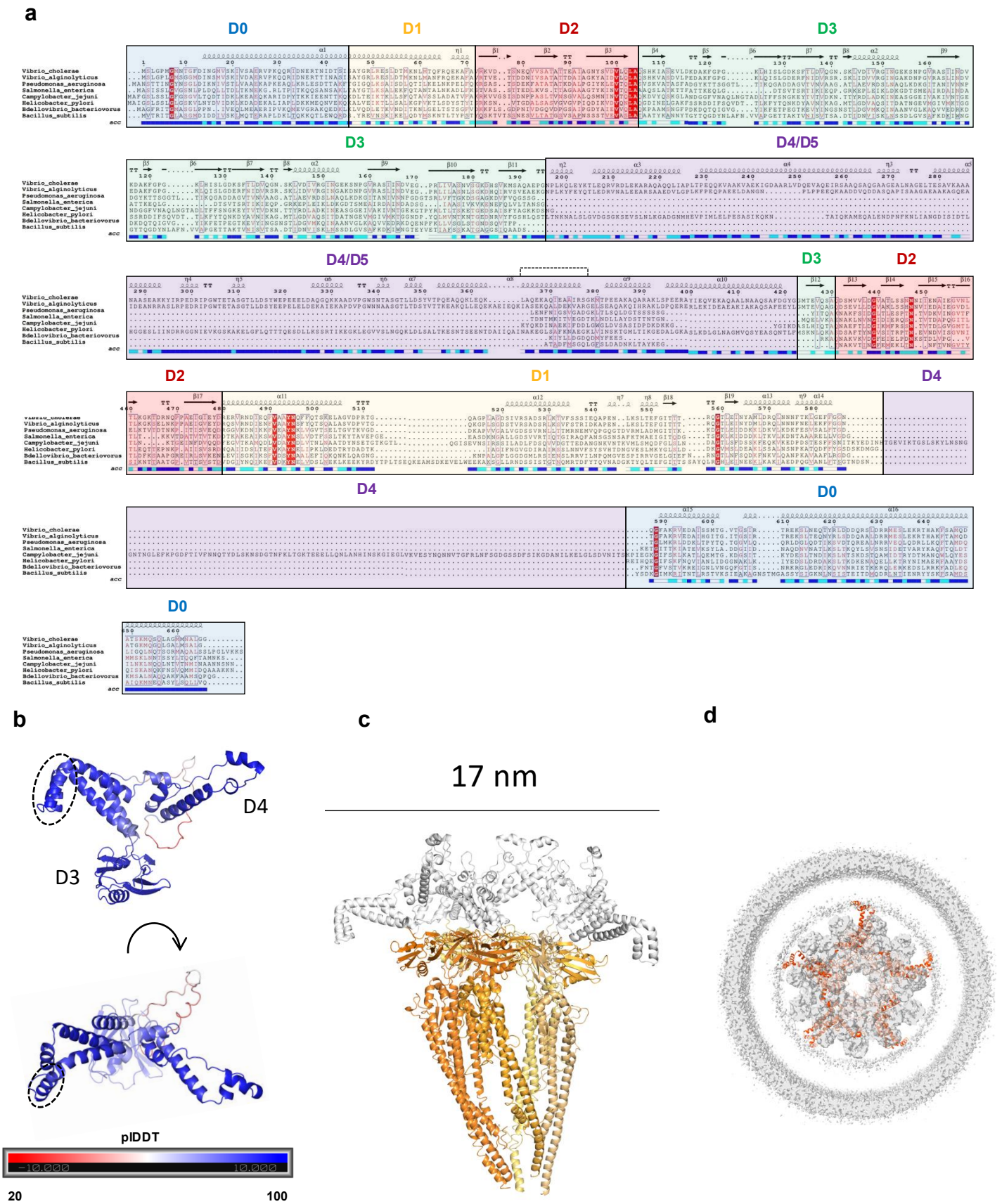

Figure S7. Multiple sequence alignment between FliD homologues and cap characteristics of FliD of *V. alginolyticus*. **a**, Multiple sequence alignment for FliD from different species. The domains are colour coded as follows: Blue: D0 terminal domains. Yellow: D1. Red: D2 domain. Green: D3 domain. Purple: D3 domain. **b**, Alphafold prediction of the D3 and D4 domain of FliD of *V. alginolyticus* coloured acording to the pIDDT score. **c**, Dimensions of the predicted FliD D4 domain structure of *V. alginolyticus*. **d**, Overlay of the cross-view 3D reconstruction of the sheathed filament (grey) and the top-view of the FliD D4 domain model (orange) of *V. alginolyticus.* The diameter of the D4 domain of FliD and the inner leaflet of the sheath are similar.

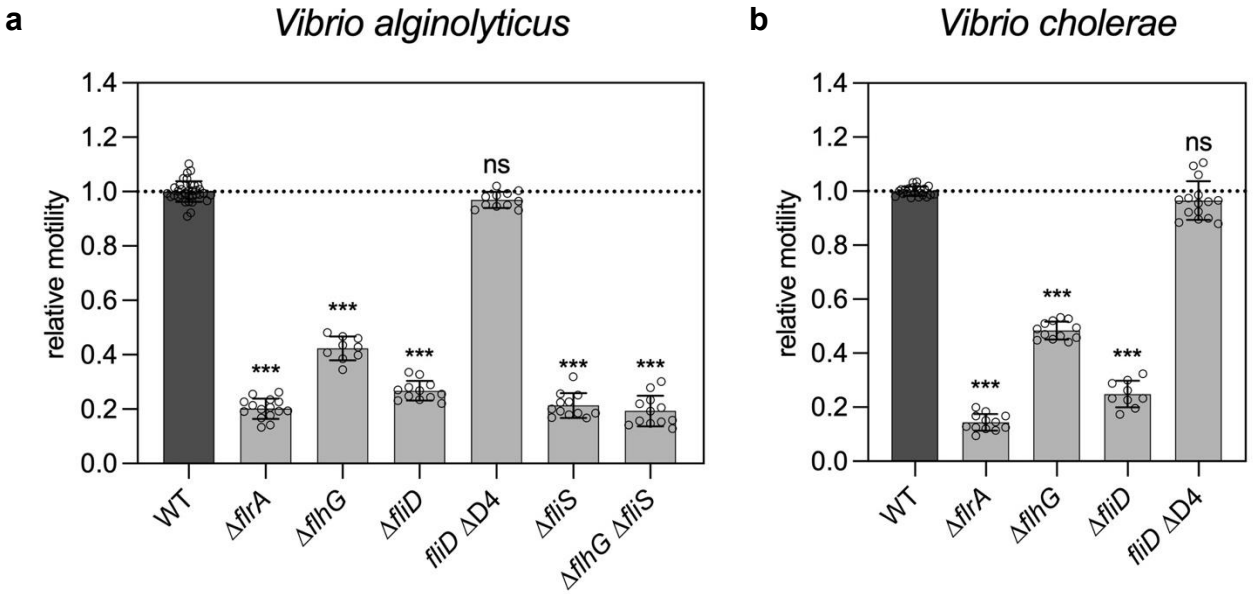

Figure S8. Motility assays for the various mutants employed to characterize flagellum assembly. **a**, Relative motility of *V. alginolyticus* mutants, analyzed using soft-agar motility plates after 6-8 h incubation at 37 °C. **b**, Relative motility of *V. cholerae* mutants, analyzed using soft-agar motility plates after 6-8 h incubation at 37 °C.

Motility halos were measured using Fiji and normalized to the WT. Bar graphs show mean ± SD from ≥3 biological replicates with individual data points. Statistical analysis was performed using one-way ANOVA followed by Dunnett's multiple comparisons test (GraphPad Prism). *, $p < 0.05$; **, $p < 0.01$; ***, $p < 0.001$; ns, non-significant.

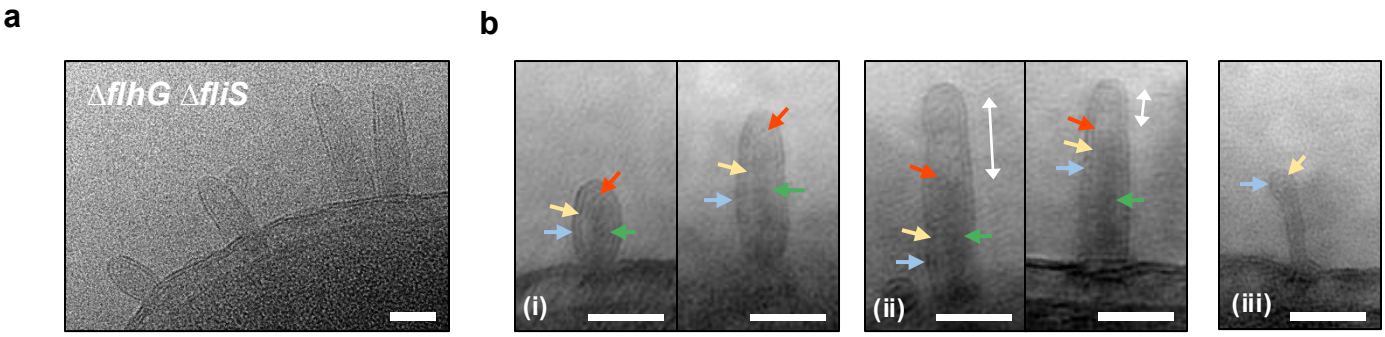

Figure S9. Position of cap complexes at early stages of filament assembly. a, Slice of a representative cryo-electron tomograph of a hyperflagellated *V. alginolyticus* strain with impaired flagellin secretion (Δ*flhG* Δ*fliS*). **b**, close-up views showing distinct flagellar architectures in which the (i) cap complex is located near the sheath, the (ii) filament is shorter and the cap is located below the sheath and (iii) empty sheath without a filament. Arrows indicate the membrane outer later (blue), inner layer (yellow), filament (green) and cap (orange).